

Investigation of the Ability of the Corrosion Protection of Zn-Mg Coatings

Hana Ferkous¹, Brahim Talhi², Mohammed Barj³, Rabah Boukherroub¹ and Sabine Szunerits^{*1,4}

¹*Institut de Recherche Interdisciplinaire (IRI, USR-3078) and Institut d'Electronique, de Microélectronique et de Nanotechnologie (IEMN, CNRS-8520), Cité Scientifique, Avenue Poincaré – B.P. 60069, 59652 Villeneuve d'Ascq, France*

²*Laboratoire de Corrosion Université Badji Mokhtar BP 12 – 23000, Annaba, Algérie*

³*Laboratoire de Spectrochimie Infrarouge et Raman (LASIR, UMR 8516), Bât C5, 59655 Villeneuve d'Ascq, France*

⁴*Laboratoire d'Electrochimie et de Physicochimie des Matériaux et des Interfaces (LEPMI), CNRS-INPG-UJF (UMR 5631), 1130 rue de la piscine, BP 75, 38402 St. Martin d'Hères Cedex, France*

Abstract: Presently Zn-Mg coatings are being developed as a contribution to next generation of galvanized steel. However, the underlying corrosion mechanism is still under debate. In this paper we show that Raman spectroscopy next to electrochemical methods (linear sweep voltammetry and electrochemical impedance spectroscopy) can successfully be used to help in identifying the corrosion products of Zn-Mg coated galvanized steel (ZMS) when dipped into 3 wt. % NaCl aqueous solution at ambient temperature (25 °C). The obtained results are compared to galvanized steel. This study reveals that in the case of ZMS, Mg is mainly anodically dissolved forming a compact layer of Mg(OH)₂/MgO and MgCO₃. It is believed that the formation of this compact layer and the insulating properties of MgO, due to its large band gap, are responsible for the increased corrosion resistance of the alloy.

Keywords: Zn, Zn-Mg, sodium chloride, impedance spectroscopy, corrosion, corrosion protection.

1. INTRODUCTION

The use of steel construction materials with long life time is mainly possible due to the use of protective metallic coatings containing zinc. The protective nature of Zn-coated or galvanized steel is linked to the formation of a thick and porous film of Zn corrosion products, which influence the reduction mechanisms and rate of oxygen on the zinc surface. To extend the life time of steel construction, big efforts have been put into the optimization of Zn coating composites. One attempt to improve the protective ability of zinc-coated steel is to developed alloys [1-5]. Magnesium-based alloys are promising alternatives as they exhibit a number of advantageous physical and mechanical properties that make them attractive for many industrial applications [6, 7]. Presently Zn-Mg coatings are developed by the steel industry as they are believed to be the next generation of galvanized steel [8]. Several different reports have highlighted the increased corrosion resistance of Zn-Mg over Zn-coated steel [8-11].

Zinc corrosion and dissolution can be easily studied by electrochemical methods, allowing the determination of corrosion rates and reaction models [12-18]. As corrosion is a surface process, surface characterization techniques such as Fourier transformed infrared (FT-IR) spectroscopy, Raman spectroscopy, sum frequency generation (SFG) spectroscopy, X-ray diffraction (XRD), energy dispersive X-ray spectrometry (EDXS), or X-ray photoelectron spectroscopy (XPS) can help in the analysis and quantification of the

corrosion products, helping to shed light into the underlying corrosion mechanism [1, 3, 14, 15, 19, 20].

In this paper, Raman spectroscopy together with linear sweep voltammetry and electrochemical impedance spectroscopy are used to determine the corrosion products formed from a Zn-Mg alloy with 10 wt. % Mg when immersed in an aqueous solution of 3 wt. % sodium chloride.

2. EXPERIMENTAL SECTION

2.1. Materials

Sodium Chloride (NaCl) was obtained from Aldrich and used without further purification. Galvanized steel samples were kindly provided by Arcelor-Mittal. The Zn-Mg coating was produced by over-coating galvanized steel with magnesium *via* physical vapour deposition. The interface was subsequently thermally treated to alloy the zinc and magnesium. The final coating was 10 μm thick and contained 10 wt. % Mg.

2.2. Instrumentation

Electrochemical Instrumentation

Electrochemical experiments were performed using an Autolab potentiostat 30 (Eco Chemie, Utrecht, The Netherlands). The working electrode was galvanized steel or the Zn-Mg alloy, degreased with acetone and washed with water before use. The active surface area was $A = 0.196 \text{ cm}^2$. The disk shaped samples were mounted in a PTFE holder with copper contact. The reference electrode was saturated calomel electrode (SCE), and a platinum wire was used as a counter electrode. Measurements were performed in an aqueous solution containing 3 wt. % NaCl.

*Address correspondence to this author at the Institut d'Electronique, de Microélectronique et de Nanotechnologie (IEMN, CNRS-8520), Cité Scientifique, Avenue Poincaré-B.P. 60069, 59652 Villeneuve d'Ascq, France; E-mail: sabine.szunerits@lepmi.inpg.fr

Linear voltammetry polarization tests were performed at a rate of 1 mV s^{-1} . The cathodic and anodic fields were recorded separately.

Electrochemical Impedance Spectroscopy (EIS) was performed for eight frequency decades from 1 mHz to 100 kHz with an amplitude of 10 mV at the corrosion potential (E_{corr}). Impedance data were modeled using ZView.

AFM Measurements

The samples were imaged with a Dimension 3100 model AFM (Veeco, Santa Barbara, CA) equipped with a Nanoscope IV controller (Digital Instruments) under ambient conditions. Single beam silicon cantilevers (AFM-TM Arrow, Nanoworld) with spring constants of $\approx 42 \text{ N m}^{-1}$ and resonant frequencies of $\approx 250 \text{ kHz}$ were used. All AFM images were acquired in tapping mode at a constant force of 5–50 pN.

Scanning Electron Microscopy (SEM)

SEM images were obtained using an electron microscope ULTRA 55 (Zeiss, France) equipped with a thermal field emission emitter, three different detectors (EsB detector with filter grid, high efficiency In-lens SE detector, Everhart-Thornley Secondary Electron Detector) and an energy dispersive X-ray analysis device (EDS analysis).

Raman Spectroscopy

Raman measurements were performed using a Renishaw's InVia Raman spectrometer. Spectra were recorded with the green line of an Ar-ion laser ($\lambda = 514.53 \text{ nm}$) using a $50\times$ ($\text{NA} = 0.95$) objective. The acquisition time was 500 seconds with an output laser power of 0.5 mW.

3. RESULTS AND DISCUSSION

3.1. Electrochemical Investigations

It is well known that the surface roughness has an important influence on the anodic dissolution of Zn [16]. Fig. (1) shows the AFM images of galvanized steel (GS) and galvanized steel coated with a $10 \mu\text{m}$ thick layer of Zn-Mg (ZMS). The interfaces show comparable surface roughness with RMS values of 5.3 for GS and of 6.8 for the Zn-Mg coated interface.

Both interfaces were immersed in an aqueous solution containing 3 wt. % NaCl ($\text{pH} = 7.0$) and the evolution of the corrosion potential (E_{corr}) was followed over time. The initial corrosion potential of Zn and Zn-Mg are almost the same [11]. In the case of the Zn sprayed surface, the corrosion potential rapidly moves in the noble direction within several days due to the formation of porous corrosion products decreasing the anodic current. Indeed, E_{corr} is determined by both the anodic and cathodic reactions. A decrease of the anodic current moves E_{corr} gradually in the positive direction so that the cathodic current can be low enough to balance the decreased anodic current. For Zn-Mg sprayed surfaces the corrosion potential stayed in less noble corrosion potential regions for up to a month (Fig. 2). The slow but steady increase in E_{corr} of the interface covered with Zn-Mg indicates the formation of a protecting layer over time, which limits further dissolution of the alloy and results in an increased corrosion resistance. The superior corrosion resistance of

ZMS may be due to three factors: (i) the formation of a dense, adherent layer of Zn corrosion products on the surface or (ii) the formation of a dense and insulating layer of Mg corrosion products or (iii) the persistence of galvanic protection of the ZMS coating during corrosion. Linear sweep voltammetry (LSV) and electrochemical impedance spectroscopy (EIS) were used next to Raman spectroscopy to elucidate this question.

Quasi-steady state polarization curves of galvanized steel and ZMS are shown in Fig. (3). In the case of galvanized steel, a linear region is observed in the cathodic part of the polarization curve when immersed in an aqueous solution containing 3 wt. % NaCl. This plateau is attributed to the charge transfer due to the reduction of oxygen dissolved in the solution (equation 1). Anodically from E_{corr} , the current density increases steadily due to the anodic dissolution of zinc (equation 2).



The addition of magnesium to zinc decreases the cathodic and anodic currents and shows a more complex reduction behavior (Fig. 3). The corrosion current densities (j_{corr}) were estimated from the polarization curves through the Tafel polarization method. Galvanized Zn shows a corrosion current density of $j_{\text{corr}} = 213 \mu\text{A cm}^{-2}$ with $E_{\text{corr}} = -1.19 \text{ V}$, while a $j_{\text{corr}} = 74 \mu\text{A cm}^{-2}$ and a while $E_{\text{corr}} = -1.24 \text{ V}$ was determined for ZMS. The change in the position of the corrosion potential together with the change in the corrosion current density is most likely due to anodically formed corrosion products. The presence of Mg increases the cathodic overpotential necessary to reduce oxygen. This indicates indirectly the formation of a diffusion barrier due to the formed corrosion products, limiting the transportation of dissolved oxygen to the electrode surface.

EIS was in addition performed on galvanized Zn and ZMS samples after being immersed for 30 days in an aqueous 3 % NaCl solution. One time constant can be distinguished in the phase diagram in Fig. (4A) resulting in the proposed equivalent circuit as described in Fig. (4B). R_s corresponds to the electrolyte resistance, Q_{dc} presents the double layer capacitance and R_{ct} the charge transfer resistance. The electrolyte resistance is measured at high frequencies (10^4 – 10^5 Hz) and a value of $R_s = 43 \pm 4 \Omega \text{ cm}^{-2}$ was determined. The charge transfer resistance of galvanized steel was $R_{\text{ct}} = 2679 \Omega \text{ cm}^{-2}$ and increased significantly for ZMS to $R_{\text{ct}} = 6309 \Omega \text{ cm}^{-2}$. The double layer capacitance is as well increased from $Q_{\text{dc}} = 4.9 \Omega \text{ cm}^{-2}$ for galvanized steel to $Q_{\text{dc}} = 13 \Omega \text{ cm}^{-2}$ for ZMS. This indicates the formation of dense corrosion products protecting the interface and are in agreement with the LSV results

3.2. Raman Spectroscopy

Even though Raman spectroscopy provides weak signals, it is an easy and useful approach to identify the corrosion products formed. The vibrational properties of the corrosion products of GS and ZMS after dipping in 3 wt. % NaCl were investigated using Raman spectroscopy at 514.53 nm. The power of the illumination was as low as 0.5 mW to prevent any transformation of the materials and corrosion products

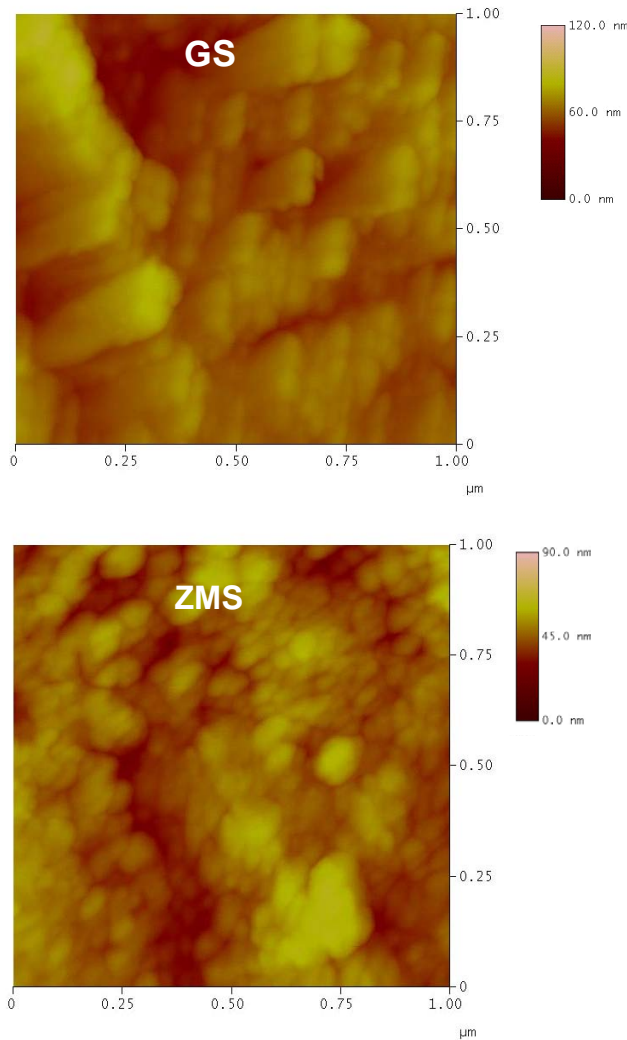


Fig. (1). AFM images of galvanized steel (GS) and galvanized steel coated with a 10 μm thick Zn-Mg layer with 10 wt. % Mg (ZMS).

formed [21]. Fig. (5) shows the Raman spectrum of galvanized steel recorded after 30 days immersion in an aqueous solution of 3 wt. % NaCl. Raman images were recorded on different parts of the sample but the same spectrum was obtained. The spectrum in Fig. (5) is thus representative of the entire corroded galvanized steel sample. Several Raman active modes are detected in the 200-3800 cm^{-1} spectral region. The Raman spectrum of corroded GS samples is dominated at low wavenumbers by the longitudinal optical (LO) vibration at $\approx 554 \text{ cm}^{-1}$ and transversal optical (TO) mode at $\approx 395 \text{ cm}^{-1}$ (E_1 symmetry) identical to that of ZnO [19, 22, 23]. ZnO can be formed during Zn corrosion, when zinc is oxidized at anodic sites to zinc ions (equation 3). The reaction is balanced by oxygen reduction at cathodic sites, producing hydroxyl anions (equation 1), which can react with zinc cations to form zinc hydroxide. In slightly acidic and alkaline solutions, thermodynamically more stable zinc oxide can precipitate onto the surface.

The peaks at longer wavenumbers, 2874 and 3482 cm^{-1} , are characteristic of hydroxyl groups of simonkolleite structure, $\text{Zn}_5(\text{OH})_8\text{Cl}_2 \cdot \text{H}_2\text{O}$ [19]. In the presence of high concentration of sodium chloride, chloride and hydroxyl anions

migrate to anodic zinc dissolution sites where simonkolleite is formed according to equation 4. The SEM image of the corroded galvanized steel interface shows the formation of flower-like structures, which are in agreement with the formation of simonkolleite (Fig. 6) [15]. Simonkolleite is not stable under alkaline conditions. The released hydroxyl ions can be neutralized by cathodic activity according to equation 5 to yield zincate ions.

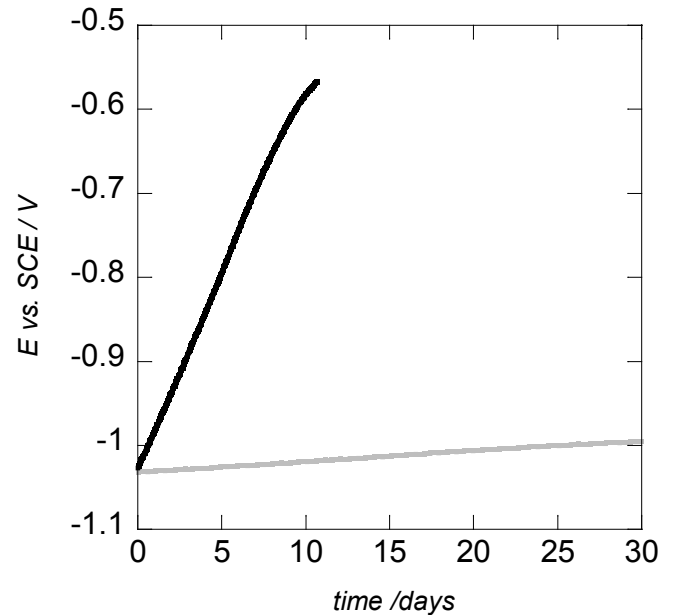


Fig. (2). Evolution of open circuit potential vs time of galvanized steel (black) and Zn-Mg coated galvanized steel (grey) dipped in a 3 wt. % NaCl aqueous solution.

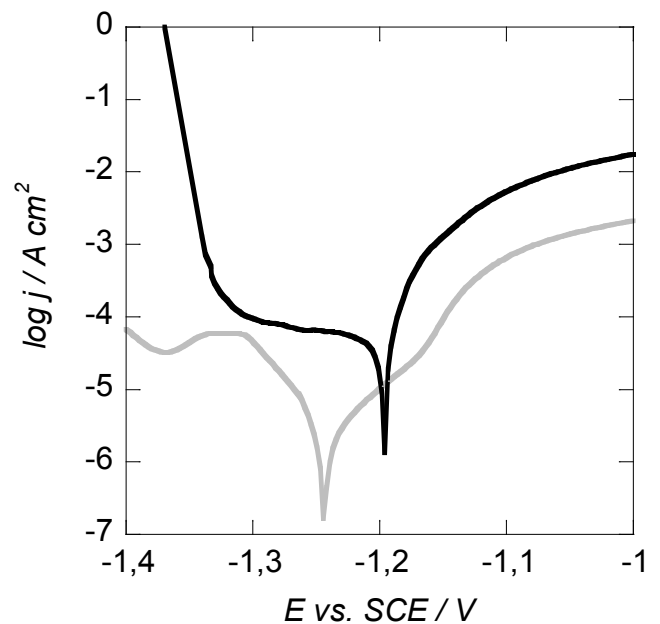


Fig. (3). Linear polarization curves of galvanized steel Zn (black line), and ZMS (grey line) after immersion in 3 % NaCl aqueous solution.

Indeed, the Raman bands at 280 cm^{-1} and 432 cm^{-1} are characteristic for brucit and MgO [24]. In contrast to ZnO, which has n-type semiconducting properties with a band gap of 3.4 eV, MgO has a higher band gap of 7.7 eV. This larger

band gap will result in a reduced efficiency of the oxygen reduction at the surface. The overall result is that once MgO is formed, the conductivity of the samples is smaller and thus less efficient in terms of oxygen reduction. A similar interpretation was given by Prosek *et al.* who studied the corrosion mechanism of Zn-Mg alloys in atmospheric conditions [9]. The band at 555 cm^{-1} indicates that ZnO is present next to brucite and MgO as one of the corrosion products. At longer wavenumbers, broad Raman peaks were recorded at 2911 and 3665 cm^{-1} , suggesting the presence of OH groups in form of water coming most likely from $\text{Mg}(\text{OH})_2$ [25]. The bad defined band at 1087 cm^{-1} is most likely due to the formation of a small amount of (hydroxy)carbonates [21]. This indicates that corrosion products such as magnesite, MgCO_3 , nesquehonite $\text{Mg}(\text{HCO}_3)(\text{OH})\times 2\text{H}_2\text{O}$ as well as hydrozincite, $\text{Zn}_5(\text{OH})_6(\text{CO}_3)_2$ are formed in small quantities. The Raman signal at 1522 cm^{-1} is characteristic to the formation of amorphous aromatic residues and could be an artifact of the Raman investigations through local heating. Investigation of Zn-Mg alloys using FTIR spectroscopy showed similar results [9]. EDX analysis of Zn-Mg coated galvanized steel shows that while the magnesium content decreases, the amount to Zn remains constant. No chloride or sodium atoms were formed, which rules out the formation of $\text{Zn}_5(\text{OH})_8\text{Cl}_2\times\text{H}_2\text{O}$. The amount of oxygen is slightly increased, indicating that $\text{Mg}(\text{OH})_2$ is formed preferentially next to some MgCO_3 and $\text{Mg}(\text{HCO}_3)(\text{OH})\times 2\text{H}_2\text{O}$. SEM images of the ZMS before and after dipping in 3 wt. % NaCl aqueous solution are displayed in Fig. (6). A granular structure is seen for the Zn-Mg film, which is covered with a dense layer of corrosion products.

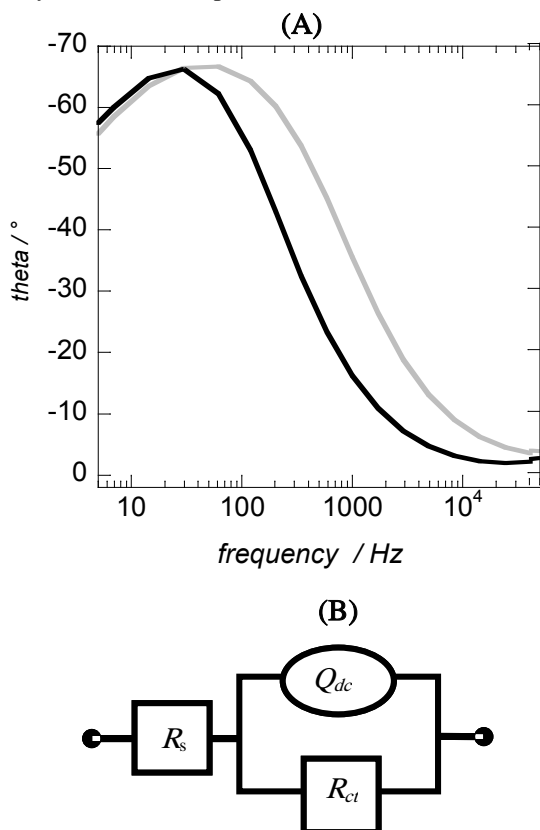


Fig. (4). (A) Phase diagram of galvanized steel (black) and ZMS (grey) when immersed in 3 % NaCl aqueous solution; (B) equivalent circuit.

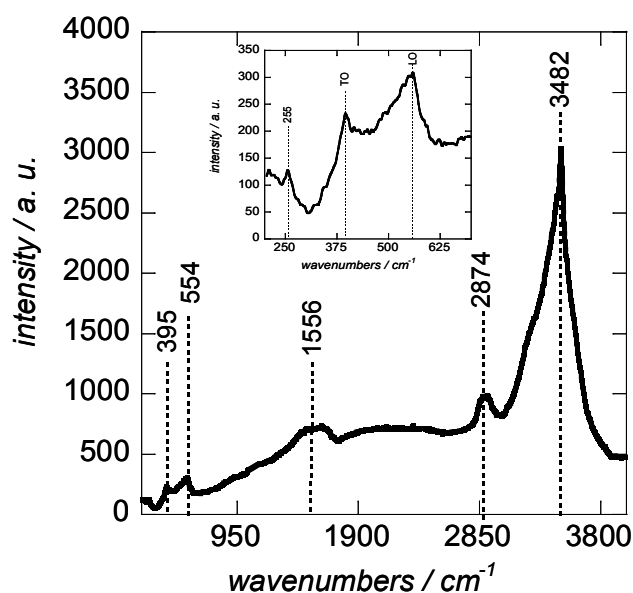
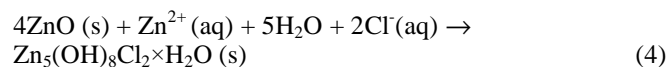


Fig. (5). Raman spectrum obtained on galvanized steel (GS) after immersion in 3 wt. % NaCl aqueous solution for 30 days.



The results of EDX analysis of corroded galvanized steel are summarized in Table 1. After dipping GS in a 3 wt. % NaCl aqueous solution, the amount of oxygen increased. Additional peaks due chloride, sodium and carbon elements were observed on the surface. This is a further indication for the formation of zinc oxide and simonkolleite as main corrosion products. The presence of sodium ions indicates the formation of Na_2CO_3 due to dissolved CO_2 in the electrolyte (equations 6, 7):

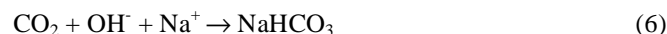


Table 1. EDX Results (wt %) of the Galvanized Steel (GS) and Coated with Zn-Mg Before and After Immersion for 30 min in an Aqueous Solution of 3 wt. % NaCl

Interface	Zn	Mg	C	O	Cl	Na
GS	99.99	-	-	0.01	-	-
GS after Corrosion	53.63	-	2.45	23.61	7.73	12.58
ZMS	85.63	9.84	0.74	3.79	-	-
ZMS after Corrosion	84.84	7.09	0.82	7.25	-	-

The Raman spectra of the ZMS dipped in 3 wt. % NaCl aqueous solution are rather different to that of GS. Fig. (7) shows the kind of spectra, which were recorded on different areas of the ZMS interface. The form and position of the Raman bands are different from that of corroded galvanized steel. In the low wavenumbers range, Raman bands at 280 cm^{-1} , 555 cm^{-1} with a shoulder at a lower wavenumber ($\approx 432\text{ cm}^{-1}$) are observed. One of the corrosion products possi-

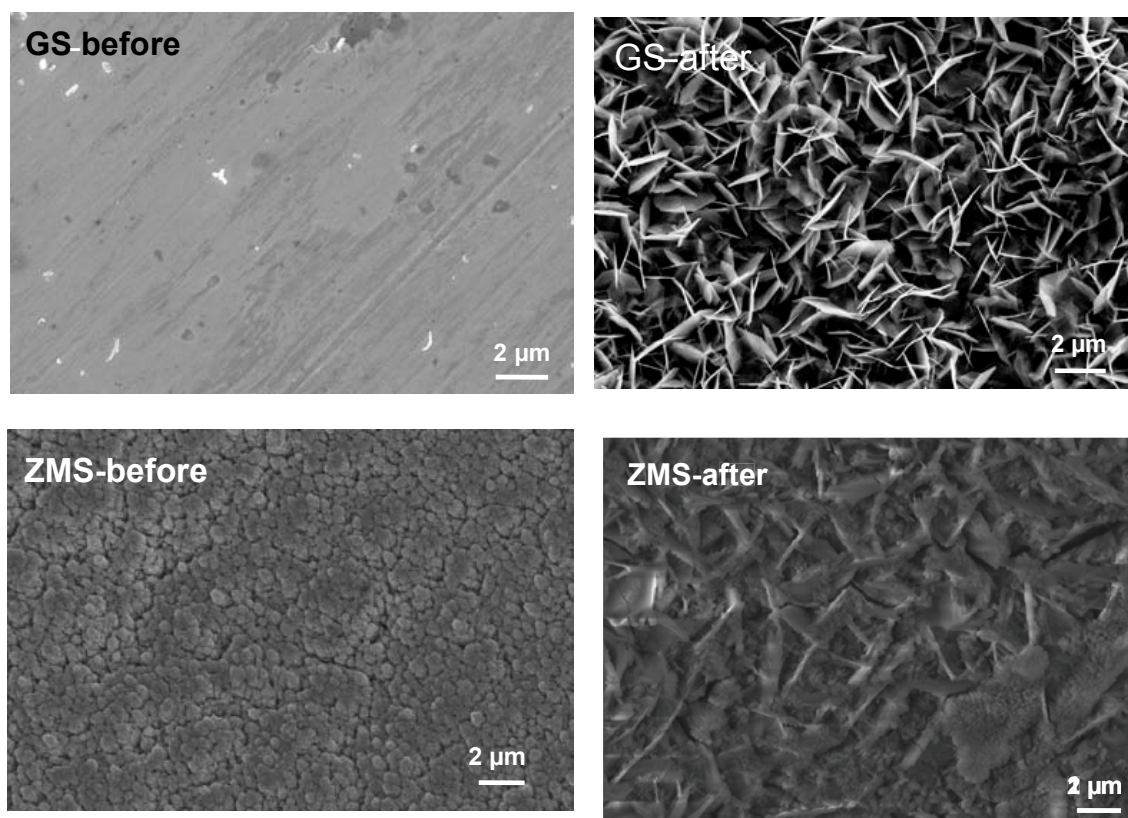


Fig. (6). SEM images of galvanized steel (GS) and Zn-Mg coated galvanized steel (ZMS) before (a) and after (b) immersion in 3 wt. % NaCl aqueous solution for 30 days.

ble of a Zn-Mg coating on galvanized steel is brucite, $\text{Mg}(\text{OH})_2$, and magnesium oxide MgO (equations 8, 9). As magnesium has a significant lower standard potential ($E^0 = -2.38 \text{ V/SHE}$) compared to Zn ($E^0 = -0.76 \text{ V/SHE}$) [26, 27], the corrosion performance of the Zn-Mg coating will be shifted in the direction of Mg and could be the driving force providing the corrosion current at the initial stage. Discharged Mg^{2+} can rapidly form a surface film of $\text{Mg}(\text{OH})_2$ or MgO , which can provide a protection over a wide pH range.



4. CONCLUSION

Raman spectroscopy was used to help in identifying the corrosion products of galvanized steel and Zn-Mg coated galvanized steel when dipped in 3 wt. % NaCl aqueous solutions. In the case of galvanized steel, the main corrosion products are $\text{Zn}_5(\text{OH})_8\text{Cl}_2 \times \text{H}_2\text{O}$ and ZnO . For Zn-Mg coated galvanized steel, Mg is mainly anodically dissolved forming $\text{Mg}(\text{OH})_2/\text{MgO}$ and $\text{MgCO}_3/\text{Mg}(\text{HCO}_3)(\text{OH}) \times 2\text{H}_2\text{O}$ as corrosion products. It is believed that the formation of a compact layer of the corrosion products of Mg is responsible for the improved corrosion resistance of Zn-Mg coated galvanized steel. LSV and EIS results point towards this interpretation. The ability to transfer electrons to the metal is thus reduced in two ways: (i) by the formation of a dense layer composed of $\text{Mg}(\text{OH})_2/\text{MgO}$ and $\text{MgCO}_3/\text{Mg}(\text{HCO}_3)(\text{OH}) \times 2\text{H}_2\text{O}$ and (ii) by the insulating properties of MgO due to its large band gap.

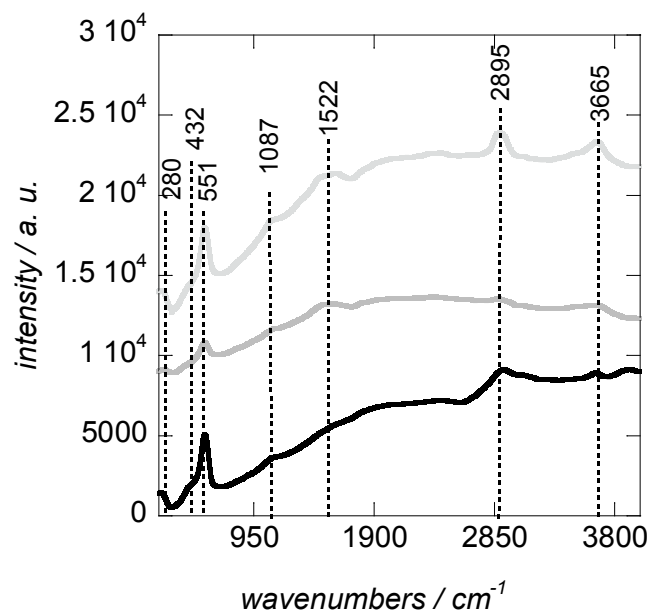


Fig. (7). Raman spectra recorded on galvanized steel coated with a Zn-Mg protection layer on three different places after immersion in 3 wt. % NaCl for 30 days.

ACKNOWLEDGEMENTS

The Centre National de la Recherche Scientifique (CNRS) and the Nord Pas de Calais region are gratefully acknowledged for financial support. HF thanks the “ministère algérien de l’enseignement supérieur” for financial sup-

port (PROFAS program). The authors want to thank Arcelor for providing the samples. The authors thank Mei Wang and Gaëlle Piret for helping with AFM and SEM imaging, respectively. We also thank P. Dornstein for Mg deposition and annealing.

REFERENCES

- [1] Boshkov N, Petrov K, Raichevski G. Corrosion behavior and protective ability of multilayer galvanic coatings of Zn and Zn-Mg alloys in sulfate containing medium. *Surf Coat Technol* 2006; 200: 5995.
- [2] Boshkov N, Petrov K, Vitkova S, Nemska S, Raichevsky G. Composition of the corrosion products of galvanic alloys Zn-Co and their influence on the protective ability. *Surf Coat Technol* 2002; 157: 171.
- [3] Dubent S, De Petris-Wery M, Saurat M, Ayedi HF. Composition control of tin-zinc electrodeposits through means of experimental strategies. *Mat Chem Phys* 2007; 104: 146.
- [4] Butefuhr M. Zinc-Aluminium-Coatings as Corrosion Protection for Steel. *Werkst Corr* 2007; 58: 721.
- [5] Sylla D, Savall C, Gadouleau M, Rebere C, Creus J, Refait PH. Electrodeposition of Zn-Mg alloys on steel using an alkaline pyrophosphate-based electrolyte bath. *Surf Coat Technol* 2005; 200: 2137.
- [6] Mathieu S, Rapin C, Steinmetz J, Steinmetz P. A corrosion study of the main constituent phases of AZ91 magnesium alloys. *Corr Sci* 2003; 45: 2741.
- [7] Lamaka SV, Montemor MF, Galio AF *et al.* Novel hydride sol-gel coatings for corrosion protection of AZ31B magnesium alloy. *Electrochim Acta* 2008; 53: 4773.
- [8] Hosking NC, Ström MA, Shipway PH, Rudd CD. Corrosion resistance of zinc-magnesium coated steel. *Corr Sci* 2007; 49: 3669.
- [9] Prosek T, Nazarov A, Bexell U, Thierry D, Serak J. Corrosion mechanism of model zinc-magnesium alloys in atmospheric conditions. *Corr Sci* 2008; 50: 2216.
- [10] Schuhmacher B, Schwerdt C, Seyfert U, Zimmer O. Innovative steel strip coatings by means of PVD in a continuous pilot line: process technology and coating development. *Surf Coat Technol* 2003; 163-164: 703.
- [11] Katoh K, Kojima K, Ishimoto H, Yashiki T. Development of corrosion preventive Zn-Mg thermal sprayed steel plate for oil storage tanks. *JHPI* 2004; 42: 207.
- [12] Deslouis C, Duprat M, Tournillon Chr. The kinetics of zinc dissolution in aerated sodium sulphate solutions. A measurement of the corrosion rate by impedance techniques. *Corr Sci* 1989; 29: 13.
- [13] Zhang XG. *Corrosion and Electrochemistry of Zinc*. Plenum Press; New York: 1996.
- [14] Cachet C, Ganne F, Maurin G, Petijean J, Vivier V, Wiart R. EIS investigation of zinc dissolution in aerated sulfate medium. Part I: bulk zinc. *Electrochim Acta* 2001; 47: 509.
- [15] Chen YY, Chung SC, Shih HC. Studies on the initial stages of zinc atmospheric corrosion in the presence of chloride. *Corr Sci* 2006; 48: 3547.
- [16] Giménez-Romero D, García-Jareño JJ, Vicente F. Correlation between the fractal dimension of the electrode surface and the EIS of the zinc anodic dissolution for different kinds of galvanized steel. *Electrochem Commun* 2004; 6: 148.
- [17] Cachet C, Wiart R. The kinetics of zinc dissolution in chloride electrolytes: impedance measurements and electrode morphology. *J Electroanal Chem* 1980; 111: 235.
- [18] Yadav AP, Nishikata A, Tsuru T. Oxygen reduction mechanism on corroded zinc. *J Electroanal Chem* 2005; 585: 142.
- [19] Marchebois H, Joiret S, Savall C, Bernard J, Touzain S. Characterization of zinc-rich powder coatings by EIS and Raman spectroscopy. *Surf Coat Technol* 2002; 157: 151.
- [20] Zhang H, Baldelli S. Alkanethiol monolayers at reduced and oxidized zinc surfaces with corrosion protection: assume frequency generation and electrochemistry investigation. *J Phys Chem B* 2006; 110: 24062.
- [21] Colomban Ph, Cherifi S, Despert G. Raman identification of corrosion products on automotive galvanized steel sheets. *J Raman Spect* 2008; 39: 881.
- [22] Tzolov M, Tzenov N, Dimova-Malinovska D, *et al.* Vibrational properties and structure of undoped and Al-doped ZnO films deposited by RF magnetron sputtering. *Thin Solid Films* 2000; 379: 28.
- [23] Damen TC, Porto SPS, Tell B. Raman effect in zinc oxide. *Phys Rev* 1966; 142: 570.
- [24] Duffy TS, Meade C, Fei Y, Mao H-K, Russell JH. High-pressure phase transition in brucite, Mg(OH)₂. *Am Mineral* 1995; 80: 222.
- [25] Pye CC, Rudolph WW. An ab initio and raman investigation of magnesium(II) hydration. *J Phys Chem A* 1998; 102: 9933.
- [26] Song G, Atrens A. Corrosion mechanism of magnesium alloys. *Adv Eng Mater* 1999; 1: 11.
- [27] Song G, Atrens A. Understanding Magnesium Corrosion. *Adv Eng Mater* 2003; 5: 837.

Received: December 15, 2008

Revised: January 20, 2009

Accepted: January 21, 2009

© Ferkous *et al.*; Licensee Bentham Open.

This is an open access article licensed under the terms of the Creative Commons Attribution Non-Commercial License (<http://creativecommons.org/licenses/by-nc/3.0/>) which permits unrestricted, non-commercial use, distribution and reproduction in any medium, provided the work is properly cited.